CROSS FLOW PAST SUCCESSIVELY POSITIONED CIRCULAR CYLINDERS

I. A. Belov and N. A. Kudryavtsev

UDC 532.517.2

The numerical scheme of A. Arakawa is used to carry out a numerical analysis of the cross flow past two successively positioned cylinders.

In the present work, we investigate the cross flow of a viscous heat-conducting incompressible fluid past two cylinders with equal radii R* (here and in what follows, the index * indicates a dimensionless quantity). The cylinders are positioned in succession in the direction of flow and are located at a quite close distance L* from one another, so that the nature of the flow past them is affected by the interaction of the perturbations that each contributes to the flow. It is assumed that the liquid has a constant velocity U_∞^* and temperature T_∞^* at infinity; the surface temperature of the cylinders T_w^* is assumed to be constant. In constructing the solution, we will neglect the effect of the possible asymmetry of the flow caused by the unstable process of wake formation. The symmetry condition for the flow in this case limits the range of Reynolds numbers to comparatively low magnitudes on the order of 30-40 according to data on flow past a single cylinder (see, e.g., [1]). In spite of the limitation indicated, it should be noted that the problem being examined is important for studying many phenomena; the results of its solution can be, in particular, used in carrying out thermal flowmeter measurements of pulsations in flow parameters.

We construct the solution in difference form using a nonstationary formulation in a polar coordinate system (r, θ), whose origin we place at the center of the first (along the flow) and second (in the wake behind it) cylinder. The region in which the calculations are carried out, bounded by the cylinder surfaces, the symmetry plane, and the surfaces far away from the cylinders on which the unperturbed flow conditions or conditions for continuation of the solution ("soft" conditions) are satisfied, is separated into two subregions, connected to the first and second cylinders (Fig. 1). We used the exact Navier—Stokes equations in the form of the vortex transport equation in vorticity ω and stream function ψ variables, and the energy equation relative to the static flow temperature T. In the transformed system of coordinates (ξ, θ), where $\xi = \ln(r)$, the starting system of equations in dimensionless form is written as follows:

$$-\omega = \exp(-2\xi)\,\Delta\psi; \tag{1}$$

$$-\exp(2\xi)\frac{\partial f}{\partial t} + I + \frac{2}{\mathrm{RePr}^{\gamma}}\Delta f = 0, \tag{2}$$

where $f \equiv \omega$, $\gamma = 0$ for the vortex transport equation; $f \equiv T$, $\gamma = 1$ for the energy equation; I represents the convective terms; $\Delta = \partial^2/\partial\xi^2 + \partial^2/\partial\theta^2$.

In (1) and (2), the radius of the cylinder R* and the velocity U_∞^* are used as characteristic quantities: the dimensionless temperature is related to the dimensional temperature by the following relation $T = (T^* - T_\infty^*)/(T_w^* - T_\infty^*)$. The Reynolds (Re) and Prandtl (Pr) numbers, as well as the local Nusselt (Nu) number determined during the calculation, are represented in the form $\mathrm{Re} = 2R^*U_\infty^*/\nu^*$; $\mathrm{Pr} = \nu^*/a^*$; $\mathrm{Nu} = 2R^*\alpha^*/\lambda^*$. Evidently, the local Nusselt number is expressed in terms of the temperature gradient on the cylinder surface $\mathrm{Nu} = -2(\partial T/\partial r)_w$.

In replacing system (1) and (2) by its difference analog, we will use A. Arakawa's second-order scheme in approximating the convective terms I [2]. Experience in using this scheme shows that it is possible to obtain a stable solution of the Navier—Stokes equations over a quite wide range of Re numbers, when the difference approximation of the time

Mechanical Institute, Leningrad. Translated from Inzhenerno-Fizicheskii Zhurnal, Vol. 41, No. 2, pp. 310-317, August, 1981. Original article submitted June 23, 1980.

 0022-0841/81/4102-0900$07.50

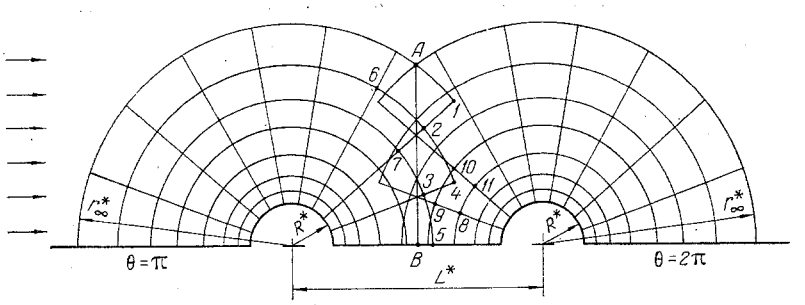

Fig. 1. Computational region and difference grid.

derivatives also has second-order accuracy. This is attained here by centering the time derivatives $\partial f/\partial t$.

Let us formulate the boundary conditions for the computational region indicated in Fig. 1. First we will consider the conditions that are identical for the first and second subregions.

We assume that $\psi_w = 0$ on the cylinder surface ($\xi = 0$). Solving Eq. (1) and using the linear representation for ψ in the vicinity of the wall, we obtain for the vorticity on it

$$\omega_w = -2\psi_{w+1}/h^2, \tag{3}$$

where ψ_{w+1} is the stream function of the layer of the difference scheme closest to the cylinder; h is the grid step. For the wall temperature, we have $T_w = 0$. On the symmetry axis ($\theta = \pi$, 2π), $\psi = \omega = \partial T/\partial\theta = 0$. On the outer boundary of the computational region, taking into account the fact that the flow here is unperturbed, we obtain $\omega = T = 0$; $\psi = r_\infty \sin\theta$, where $r_\infty = \exp(\Sigma)$ is the radial distance from the center of the cylinder to the external boundary of the computational region; Σ is the value of ξ, corresponding to $r = r_\infty$.

Due to the mutual effect of the cylinders on one another, we introduce into the analysis the following additional boundary conditions, taking into account this influence. The essence of the formulation of these conditions lies in the fact that among the inner nodes of the computational subregions, we separate out nodes which are then considered as boundary nodes in the computational process. As an illustration, we will show how the boundary nodes are constructed and how the conditions of them are determined for the first computational subregion (Fig. 1).

1. We construct the line AB perpendicular to the axis of symmetry, centered between the centers of the cylinders (the point A lies on the intersection of the external boundaries, and B lies on the axis of symmetry).

2. For each radial coordinate grid line in the first computational subregion, intersecting AB, we determine the node that is closest to the line AB and lies to the right of it (for example, nodes 2, 3, and 5). If such nodes lie on different circles for neighboring radii, then we add the required number of nodes so that the nodes located within the field of the first computational subregion are completely defined in accordance with the computational scheme adopted. We find that it is necessary to add nodes 1 and 4 to the boundary nodes that we already have.

3. Each boundary node of the first computational subregion must fall into some cell of the second computational subregion. Thus, boundary node 4 is located in the cell formed by nodes 8, 9, 10, and 11. Then, the variables at node 4 are determined as follows with the help of linear interpolation:

$$f_4 = l_8 f_8 + l_9 f_9 + l_{10} f_{10} + l_{11} f_{11},$$

where l_i are the interpolation coefficients, which remain unchanged during the computation; $f \equiv \psi$, ω, and T.

Similar relations, constructed for each boundary node (except the fifth node, where the flow parameters are obtained from the symmetry conditions), completely determine for the first computational subregion the boundary conditions sought, constructed taking into account the effect of the perturbations introduced by the second cylinder.

The boundary conditions for the flow parameters in the section where the solutions for the first or second subregions are joined can then be written in the following generalized form

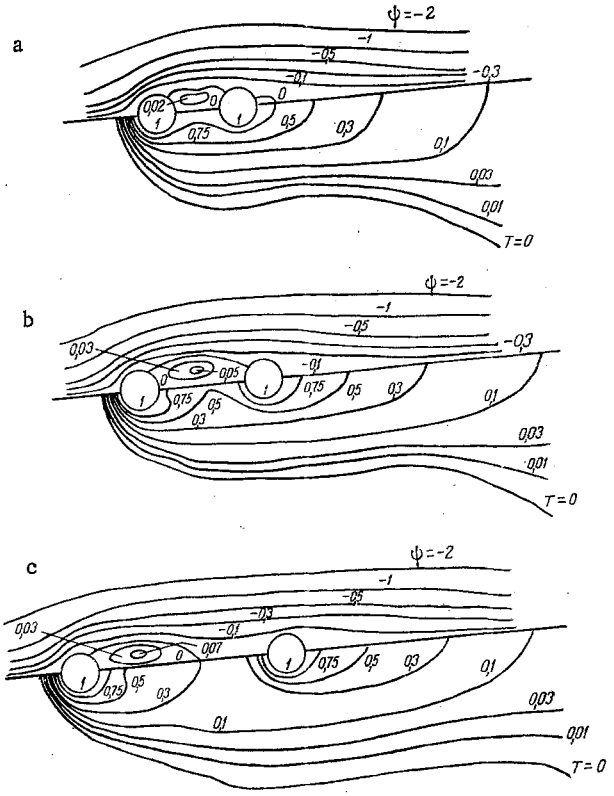

Fig. 2. Lines of constant values of the stream function (above) and temperature (below) for the following values of the distances between the cylinders: a) L = 4; b) L = 6; c) L = 10.

$$f_j = \sum_{i=1}^{4} l_i f_i, \tag{4}$$

where j indicates any boundary node in the first or second subregions, and the sum is taken over the product of the interpolation coefficients and the corresponding parameters $f \equiv \psi$, ω, and T at the nodes of the second or first subregions, surrounding node j.

The numerical procedure provides for separate solution of the dynamic and heat problems. First, the stream and vorticity function fields are calculated in the following order:

1) the initial conditions for the stream and vorticity functions are given in both computational subregions ($\psi = \omega = 0$);

2) ψ and ω are calculated at the boundary nodes of the first computational subregion in accordance with (4);

3) an iterative procedure is used for solving (1) in the first computational subregion;

4) the vorticity ω_w is determined on the surface of the first cylinder according to (3);

5) the vorticity field is found from (2) for the first computational subregion at the first time step;

6) ψ and ω are computed at the boundary nodes of the second computational subregion according to (4);

7) an iteration procedure is used for solving (1) in the second computational subregion;

8) the vorticity ω_w is determined on the surface of the second cylinder according to (3);

9) the vorticity field is found from (2) for the second computational subregion at the first time step;

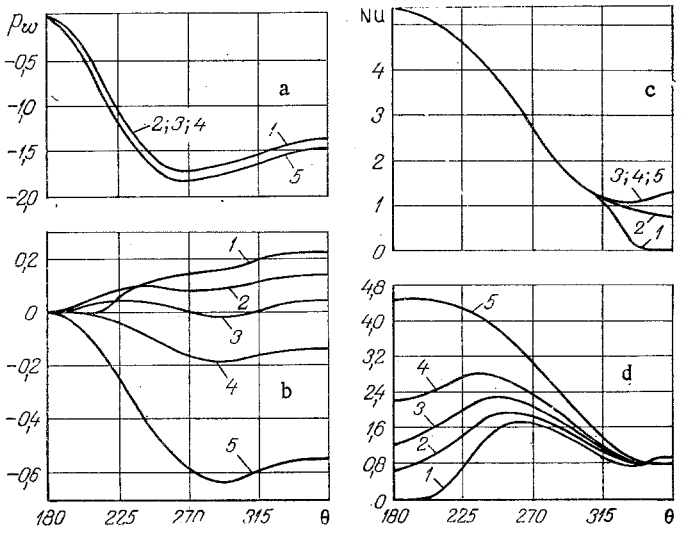

Fig. 3. Pressure distribution (a, b) along the surface of the cylinder and distribution of the local Nusselt number (c, d) on the surface of the cylinder (a, c correspond to the first cylinders; b, d correspond to the second one): 1) L = 2; 2) L = 4; 3) L = 6; 4) L = 10; 5) L = 20. θ is in degrees.

10) the values of ψ and ω obtained for both computational subregions are used as initial values, and the entire computational process, beginning with the second point, is repeated at the next time step.

The computation continues until a stationary state is reached; the criterion used for establishing the steady state is that the time derivative of the magnitudes of the drag coefficients C_x, referred to $\rho^* R^* U_\infty^{*2}$, are approximately equal to 0 for each cylinder. In a polar coordinate system, C_x is defined as the sum of the pressure drag coefficient C_{xp} and the friction drag coefficient C_{xf}, where

$$C_{xp} = -\int_{\pi}^{2\pi} p_w \cos\theta \, d\theta; \quad C_{xf} = -\frac{4}{\mathrm{Re}} \int_{\pi}^{2\pi} \omega_w \sin\theta d\theta.$$

The pressure on the surface of the cylinder p_W, referred to $\rho^* U_\infty^{*2}/2$, is determined from the equation of motion

$$p_w = \frac{4}{\mathrm{Re}} \int_{\pi}^{\theta} \left(\frac{\partial \omega}{\partial \xi} \right)_w d\theta,$$

where without loss of generality the constant of integration is set equal to zero.

After solving the dynamic problem, we proceed to the solution of the heat problem, using the field of values obtained for the stream function. The numerical procedure in this case involves determining the values of the temperature T at the boundary nodes from (4) and solving the energy equation (2) for each computational subregion successively in time. The calculation is carried out until a steady state is reached; the criterion used for the steady state is that the time derivative of the magnitude of the Nusselt number averaged over the perimeter of the cylinder approximately equals zero:

$$\mathrm{Nu}_{\mathrm{av}} = \left(\int_{\pi}^{2\pi} \mathrm{Nu} \, d\theta \right) / \pi.$$

The calculation of the symmetrical flow past two cylinders of equal size placed in series along the flow was carried out for Re = 40 and Pr = 0.7. The distances between the cylinders were L = 2, 4, 6, 10, and 20. The computational scheme was first tried out on the problem of the flow past an isolated cylinder ($L \to \infty$). Good agreement with the available

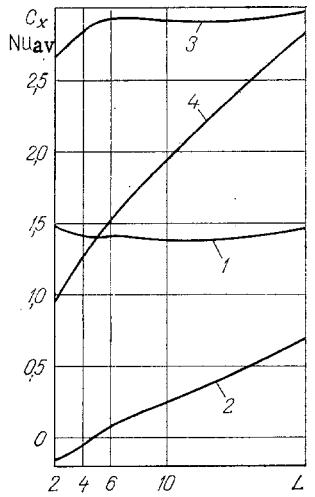

Fig. 4. Dependence of the drag coefficient and the averaged Nusselt number for the first (along the flow) and second cylinders as a function of the distance between them: 1) C_{X1}; 2) C_{X2}; 3) Nu_{av1}; 4) Nu_{av2}.

experimental and numerical results for the given problem was obtained for the following grid parameters: $h = \pi/20$; $\Sigma = \pi$; and $\Delta t = 0.05$. After carrying out a number of numerical experiments, it was established that it is preferable to use "soft" boundary conditions for the temperature $\partial T/\partial x = 0$ on the rear part of the outer boundary of the computational region ($\xi = \Sigma$; $4\pi/3 < \theta < 2\pi$). Introducing this condition permitted avoiding increasing the number of nodes in the radial direction, which otherwise would have to be done in order to obtain a convergent solution of the thermal problem. The solution of the dynamic and thermal problem of the flow past an isolated cylinder with $Re = 40$ and $Pr = 0.7$ gave $C_X = 1.62$ and $Nu_{av} = 3.15$. From experimental data [3] and numerical calculations [1, 4, 5], we have for C_X, respectively, 1.6, 1.593, 1.63, and 1.6. According to the experimental data in [6] and numerical calculations [5, 7], Nu_{av} equals, respectively, 3.17, 3.42, and 3.57. It should also be noted that quite good agreement between the computational and experimental data for the flow past an isolated cylinder was obtained for such characteristics as the distribution of pressure along the cylinder surface, the size of the wake behind the cylinder, the position of the point of flow detachment on the cylinder, and so on (see, for example, [5, 8]).

The calculation of the flow past two cylinders was carried out with the same grid parameters that were used in the case of the flow past an isolated cylinder. "Soft" conditions for the temperature were imposed on the rear part of the outer boundary for the second cylinder along the flow. Some results of the calculation are presented in what follows. Figs. 2a, b, and c illustrate the flow pattern as lines showing the constant value of the stream function and temperature for $L = 4$, 6, and 10. Figures 3a-d show the profiles of the pressure distribution and the local Nusselt number on the surface of the cylinders. Figure 4 shows the dependence of the drag coefficient C_X and the Nusselt number Nu_{av} averaged over the perimeter of a cylinder for both cylinders as a function of the distance between them.

Analysis of the computed data leads to a number of interesting observations. When the cylinders are joined ($L = 2$), a unified, more streamlined system than that of the isolated cylinder is formed. The vortex in the wake behind the second cylinder in this case is less developed, and the drag of the system is smaller in magnitude than the drag of an isolated cylinder. When the distance between the cylinders is increased ($L = 4$ and 6), a closed circulating flow forms in the space between them. In this case, there is a gradual decrease, and then complete disappearance of the circulating zone in the wake behind the second cylinder. The drag of the second cylinder remains less than zero (the effect of the drag force) up to $L \approx 4$; the total drag of both cylinders is comparable in magnitude to the drag of the isolated cylinder (the minimum in the drag of the system of cylinders is observed for $L \approx 3$; for $L \leq 6$, their drag is lower than the drag of the isolated cylinder). Further increase in the distance to $L = 10$ and 20 leads to separation of the circulating zone from the second cylinder, so that the flow past this cylinder is free of detachment. The fact that the flow past the second cylinder along the flow is free of detachment, apparently, can be explained physically in connection with the phenomenon known as the Koanda effect. Indeed, in the wake behind the first cylinder, in this case, a stream-type flow is realized with a peripheral velocity maximum. As shown in [9], in such a flow, due to the displacement of the velocity maximum from the symmetry surface of the body, liquid is sucked from the outer region directly in contact with the body past which the flow occurs (in this case, the

second cylinder) into the stream so formed. As a result, the flow in it can be less dense than in the outer region. The pressure differential formed in this case, although not large in absolute magnitude, nevertheless leads to curvature of the stream and its sticking to the cylinder. The drag of the cylinder in this case increases and becomes very close to the magnitude of the drag for an isolated cylinder; the drag of the second cylinder (as, by the way, the heat flow also) increases almost linearly with an increase in L.

An interesting practical conclusion follows from an analysis of the results presented in Fig. 4. If a performance function, characterizing maximum heat extraction for the system of cylinders for minimum system drag in the form $(Nu_{av1} + Nu_{av2})/(C_{x1} + C_{x2})$, is constructed, then the latter, as is evident from the figure, has a maximum for a distance L separating the cylinders given by $L \sim 3\text{-}4$. This distance, as follows from what has been said above, is close to the magnitude of L corresponding to the minimum drag attained by the system of cylinders in the given flow regime ($Re = 40$), when a quite well-developed circulating flow is formed in the space between the cylinders.

NOTATION

R, radius of the cylinder; L, distance between the centers of the cylinders; (r, θ), polar coordinates; (ξ, θ), transformed coordinates; U, velocity; T, temperature; ω, vorticity; ψ, stream function; p, pressure; t, time; h, step in the difference grid; Δt, time step; ν, coefficient of kinematic viscosity; a, coefficient of thermal diffusivity; α, coefficient of heat transfer; λ, coefficient of thermal conductivity; Re, Reynolds number; Pr, Prandtl's number; Nu, Nusselt number; Nu_{av}, Nusselt number averaged over the perimeter of the cylinder; I, convective terms; Δ, Laplace operator; $\gamma = 0, 1$, a coefficient that determines the form of Eq. (2); C_{xp}, pressure drag coefficient; C_{xf}, friction drag coefficient; $C_x = C_{xp} + C_{xf}$, drag coefficient; ρ, density; l, an interpolation coefficient; x, direction of the symmetry axis $\theta = 2\pi$. The indices indicate the following: *, a dimensional quantity; ∞, unperturbed flow; w, conditions at the wall; w + 1, layer closest to the wall; 1, first cylinder along the flow; 2, second cylinder along the flow; i and j, nodes in the grid.

LITERATURE CITED

1. P. C. Jain and Rao K. Sancara, "Numerical solution of unsteady viscous incompressible fluid flow past a circular cylinder," Phys. Fluids, Suppl. II, II-57—II-64 (1969).
2. A. Arakawa, "Computational design for long-term numerical integration of the equation of fluid motion: two-dimensional incompressible flow. Part I," J. Comput. Phys., 1, 119-143 (1966).
3. D. J. Tritton, "Experiments on the flow past a circular cylinder at low Reynolds numbers," J. Fluid Mech., 6, 547-567 (1959).
4. M. Kawaguti, "Numerical solution of the Navier—Stokes equations for the flow around a circular cylinder at Reynolds number 40," J. Phys. Soc. Jpn., 8, 747-757 (1953).
5. C. J. Apelt and M. A. Ledwich, "Heat transfer in transient and unsteady flows past a heated circular cylinder in the range $1 \leq R \leq 40$," J. Fluid Mech., 95, 761-777 (1979).
6. D. C. Collis and M. J. Williams, "Two-dimensional convection from heated wires at low Reynolds numbers," J. Fluid Mech., 6, 357-384 (1959).
7. S. C. R. Dennis, J. D. Hudson, and N. Smith, "Steady laminar forced convection from a circular cylinder at low Reynolds numbers," Phys. Fluids, 11, 933-940 (1968).
8. G. K. Batchelor, Introduction to Fluid Dynamics, Cambridge Univ. Press (1967).
9. L. A. Vulis and V. P. Kashkarov, Theory of Viscous Fluid Jets [in Russian], Nauka, Moscow (1965).